The Astrophysical Journal Supplement Series, 222:21 (7pp), 2016 February doi:10.3847/0067-0049/222/2/21

HIGH DYNAMIC RANGE OBSERVATIONS OF SOLAR CORONAL TRANSIENTS AT LOW RADIO FREQUENCIES WITH A SPECTRO-CORRELATOR

K. Hariharan[1], R. Ramesh[1], C. Kathiravan[1], H. N. Abhilash[2], and M. Rajalingam[1]
[1] Indian Institute of Astrophysics, Bangalore-560034, India; khariharan@iiap.res.in
[2] Poornaprajna College, Udupi-576101, India
Received 2015 February 25; accepted 2016 January 5; published 2016 February 18

ABSTRACT

A new antenna system with a digital spectro-correlator that provides high temporal, spectral, and amplitude resolutions has been commissioned at the Gauribidanur Observatory near Bangalore in India. Presently, it is used for observations of the solar coronal transients in the scarcely explored frequency range ≈30–15 MHz. The details of the antenna system, the associated receiver setup, and the initial observational results are reported. Some of the observed transients exhibited quasi-periodicity in their time profiles at discrete frequencies. Estimates of the associated magnetic field strength (B) indicate that $B \approx 0.06$–1 G at a typical frequency such as 19.5 MHz.

Key words: instrumentation: interferometers – instrumentation: polarimeters – Sun: corona – Sun: magnetic fields

1. INTRODUCTION

On a daily basis, ground-based radio spectral observations of the solar coronal transients with dedicated facilities at different locations around the globe are presently limited at frequencies $\lesssim$30 MHz (Boischot et al. 1980; Prestage 1995; Erickson 1997; Zucca et al. 2012).[3] This limits near-continuous temporal coverage of the Sun. Some of the reasons for the unavailability of such low-frequency observational facilities are the cutoff frequency for radio wave propagation in the Earth's ionosphere, and the technical difficulties related to terrestrial radio frequency interference (RFI). It would be useful if the observations were available until $\lesssim$15 MHz, as this would minimize the existing gap with observations from the space platforms at frequencies <15 MHz, and a number of related scientific problems could be investigated (see, e.g., Gopalswamy et al. 1998; Leblanc et al. 2001; Cane et al. 2002; Cane & Erickson 2005; Gopalswamy et al. 2005; Morioka et al. 2007; Eastwood et al. 2010; Gopalswamy & Mäkelä 2010; Ramesh et al. 2010b, 2011, 2012; Melnik et al. 2014; Ratcliffe et al. 2014; Carley et al. 2015; Reid & Kontar 2015). Note that presently the two spectrographs, Radio Receiver Band 1 (RAD1) and Radio Receiver Band 2 (RAD2), of the Waves experiment on board the *Wind* spacecraft, provide uninterrupted data in the frequency range ≈14 MHz–30 kHz (Bougeret et al. 1995).

Making use of the developments in the field of digital signal processing, several authors have shown that it is possible to obtain better dynamic spectra of the solar radio transients than those obtained with the conventional analog spectrum analyzers (Ebenezer et al. 2001; Ryabov et al. 2010; Iwai et al. 2012; Taylor et al. 2012; Lecacheux et al. 2014; Morosan et al. 2014). The availability of high-speed digitizers that can sample analog signals over a large bandwidth ensures simultaneous spectral coverage over the observing band during each integration time. In the case of a conventional analog spectrum analyzer, at any give time data is obtained only at a single frequency. This is because it is primarily a "sweep-frequency" instrument. The dwell period at each frequency depends on the "sweep" time between the start and end frequencies of the observing band and the number of frequency channels in the instrument, which is usually a preset parameter. The above "sweep" time also determines the time gap between the adjacent data samples at any given frequency. The larger the bandwidth of the observations, the longer the time gap will be. Note that an improvement in the temporal resolution could help us to understand the quasi-periodicity in the solar radio bursts and the related estimates of the coronal magnetic field strength (Roberts et al. 1984; Aschwanden 1987; Zhao et al. 1991; Kliem et al. 2000; Ramesh et al. 2003, 2005; ShanmughaSundaram & Subramanian 2004; SasikumarRaja & Ramesh 2013; Kishore et al. 2015). Higher spectral resolution can be used to localize the RFI in the frequency space. This helps to mark the corresponding frequency channels and the observational data in such channels are not considered for further processing (Baan et al. 2004). Similarly an increase in the number of digital bits that represent the input analog signal (i.e., the amplitude resolution) could lead to an enhancement in the the dynamic range of the observations. This could be useful for detecting weak transients in the solar atmosphere (Mercier & Trottet 1997; Ramesh & Ebenezer 2001; Ramesh et al. 2010a, 2013; Oberoi et al. 2011). That said, the advantages of digital signal processing have not been fully exploited, particularly at low radio frequencies, which offer unique diagnostics of the solar corona and the magnetic field there (see, e.g., Bastian 2004; Reiner et al. 2007; Zaqarashvili et al. 2013). One of the reasons for this is the absence of dedicated solar observing facilities at low frequencies, particularly <30 MHz. We recently commissioned a new instrument at the Gauribidanur Observatory (see Ramesh (2011) for other details related to the observatory) for observations of transient solar radio emission in the frequency range ≈30–15 MHz, with a digital spectro-correlator consisting of a high-speed analog-to-digital converter (ADC) and field programmable gate array (FPGA) hardware. Note that the correlation mode of observations provides better sensitivity (Kraus 1950). This article describes the antenna system, the associated receiver setup, the implementation of the new spectrograph, and the initial results.

[3] The Bruny Island Radio Spectrometer (Erickson 1997) has not been in operation since 2015 January (http://www.astro.umd.edu/~white/gb/).

Figure 1. View of the two LPDAs used in the spectrograph.

2. INSTRUMENT DESCRIPTION

2.1. Antenna and Analog Receiver System

We have used two log-periodic dipole antennas (LPDAs; Figure 1), designed and fabricated in-house, as the radio frequency (RF) signal receptors for the spectrograph (Duhamel & Isbell 1957; Isbell 1960; Ramesh et al. 1998; Balanis 2005; Ebenezer et al. 2007; Kishore et al. 2014). Each of them has a Voltage Standing Wave Ratio (VSWR) $\lesssim$ 2.5 over the frequency range 30–15 MHz. The half-power width of the response pattern ("beam") of the LPDAs is $\approx$100° in the *E*-plane as well as in the *H*-plane. This enables us to carry out observations for a longer time duration ($\gtrsim$6 hr) and over a wide range of declination. The effective collecting area of each LPDA is $\approx 0.3\lambda^2$, gain is $\approx$5.5 dBi, and the characteristic impedance is $\approx 50\Omega$. The above parameters are comparable to those of similar low-frequency antennas used elsewhere.[4,5] The two LPDAs have been mounted vertically with a spacing (d) $\approx$ 12 m between them on a north–south baseline. The above baseline orientation between the two LPDAs facilitates observations for a duration of $\gtrsim$6 hr without the need for steering their "beams" along the hour angle. But there will be a path length difference ($=d\sin\theta$, where θ is the zenith angle) between the RF signal incident on the two LPDAs depending on the declination (δ) of the radio source. This can be compensated either in the analog or in the digital signal path. In the analog case, a coaxial cable of appropriate length is introduced in the RF signal path from either of the two LPDAs depending on the declination of the source with respect to the local zenith. In the digital case, an instrumental time delay (τ_i) equal to the geometrical time delay $\left(\tau_g = \frac{d\sin\theta}{c}\right)$ is introduced in the appropriate signal path after the digitization and sampling of the RF signal. Note that the change in the above path length difference($=d\sin\theta$) is negligible over a $\approx \pm 3$ hr observing period of a day, for a particular declination. Also the change per day in the declination of the Sun is minimal ($\approx 0\overset{\circ}{.}1$). So the inclusion of a coaxial cable of specific length in the RF signal path will provide the required path length compensation with minimal error for about one month. Similar to the baseline between the two LPDAs, their "arms" are also oriented in the north–south direction (Figure 1). Each "arm" is essentially a $\lambda/2$ dipole and the end-to-end length of the longest "arm" is $\approx$10 m. The above separation between the LPDAs has been chosen to minimize the mutual coupling between them to < -40 dB (see, e.g., SasikumarRaja et al. 2013). The RF signal from each LPDA is passed through a high-pass filter with a cutoff frequency (f_h) $\approx$ 15 MHz (Figure 2). The filtered signal is amplified ($\approx$30 dB) and transmitted to the receiver room via a coaxial cable buried $\approx$1 m beneath the ground. The noise figure of the amplifier is $\approx$3 dB over the frequency range $\approx$30–15 MHz. The high-pass filter is used to attenuate the strong RFI at frequencies $<$15 MHz, which otherwise would saturate the amplifier and give rise to intermodulation products. A low-pass filter with a cutoff frequency (f_l) $\approx$ 30 MHz restricts the RF signal bandwidth to $\approx$30–15 MHz for further processing with the digital receiver.

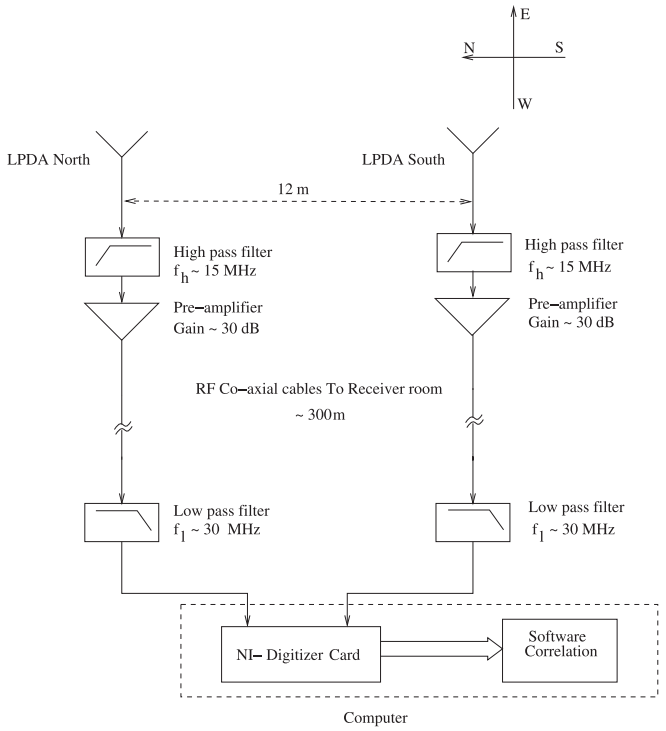

Figure 2. Block diagram of the spectrograph.

2.2. Digital Backend System

A National Instruments digitizer card (Model No. PCI-5105) is used as the backend receiver. It consists of a flash ADC and a VirtexPro-II FPGA chip based FIFO (first-in-first-out) packetizer. The number of analog input channels is eight and the maximum sampling rate is $\approx$60 MHz. In principle, an analog signal bandwidth of up to 30 MHz in the frequency range 0–60 MHz can be sampled. The FIFO has a maximum memory capacity of $\approx$128 MB (megabytes), which is shared equally by the analog input channels that are used. The card is interfaced to a computer through the conventional peripheral component interconnect (PCI) bus, which supports a maximum data transfer rate of ≈ 132 MB s^{-1}. The specifications of the above digitizer card (see Table 1) are nearly identical to that described in Ryabov et al. (2010). The LabView user interface is provided to set the control parameters of the digitizer card and the data acquisition, which involves file creating and writing

[4] http://www.lofar.org
[5] http://www.phys.unm.edu/~lwa/index.html

Table 1
Specifications of the Digitizer Card

Total number of analog *i/p* channels	8
Bit resolution	16
Sampling rate (maximum)	60 MHz
Bandwidth	30 MHz
Input voltage range (V_{pp})	0.05–30 V

operations. The data acquisition can be either in the continuous mode or in the burst mode. In either case, the on board memory is filled with the data to a specified depth during the acquisition. The data are then retrieved and stored in the hard disk of the host computer. But due to the shared on board memory and the limitations in the data transfer rate of the PCI bus, we found that there is "data overwrite" in the case of a continuous mode of operation. Hence the card is presently operated in the burst mode in which a fixed number of data samples (defined by the user) are written to the on board memory. No new acquisition will take place until all the data are retrieved. This results in a time gap of ≈10 ms between successive data acquisitions. Note that the lifetime of the solar radio transients is >1 s at low frequencies (McLean & Labrum 1985). So the above time gap should not affect the observations.

3. CORRELATION SPECTROGRAPH

Radio spectral observations of the solar corona at low frequencies are usually carried out with a single antenna (Benz et al. 2009). In order to minimize the contribution from the galactic background and improve the sensitivity, we have configured our spectrograph in the cross-correlation mode with inputs from two identical antennas. The RF signal output from the low-pass filters are connected to two of the analog input channels of the digitizer card (Figure 2). The specifications of the spectrograph are given in Table 2. The analog signals are sampled at the Nyquist rate and quantized to 16 bit data, which are then stored in the on board memory of the card. The sampled time domain data from the two antennas are then converted to the spectral domain using fast Fourier transformation (FFT). The amplitudes of each of the corresponding frequency components from the two antennas are correlated and integrated. Designating $C1$, $C2$ and $S1$, $S2$ as the cosine and sine components corresponding to the two antennas (see Figure 2) in the spectral domain, the in-phase (cosine) and quadrature (sine) correlations are estimated using the relations $X = (C1 \times C2) + (S1 \times S2)$ and $Y = (C2 \times S1) - (C1 \times S2)$, respectively (see, e.g., Ramesh et al. 2006). The visibility amplitude is given by $\sqrt{X^2 + Y^2}$. The correlated/integrated visibility amplitudes are written to the computer hard disk in binary format for further processing. The observations are carried out everyday during the interval ≈3–11 UT.

4. OBSERVATIONS

The spectrograph was commissioned in 2013 October and the data reported correspond to the period 2013 October—2014 January. A total of 71 solar radio bursts were recorded from our daily observations (see Table 4). An inspection of the dynamic spectra of the radio bursts observed with the RAD2 spectrograph on board Wind-Waves during the corresponding period indicates that all of the events listed in Table 4 continued to frequencies <15 MHz.[6]

Table 2
Specifications of the Spectrograph

Number of analog input channels	2
Frequency range	30–15 MHz
Number of frequency channels	4096
Sampling rate	60 MHz
Spectral resolution	7.32 kHz
Temporal resolution	69.6 μs

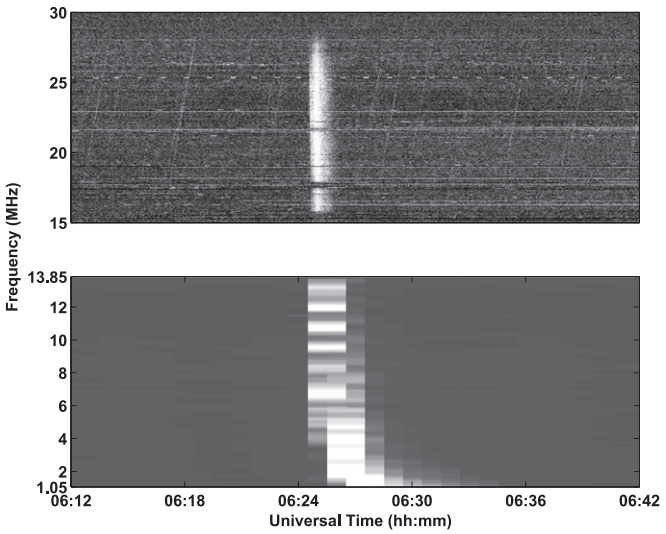

Figure 3. Upper panel: dynamic spectrum of a type III solar radio burst observed on 2013 December 14 during the interval ≈06:24–06:27 UT with the Gauribidanur low-frequency spectrograph in cross-correlation mode. One can notice that the observations are minimally affected by RFI. Lower panel: Wind-Waves RAD2 spectrograph observations of the same burst with spectral and temporal resolutions of ≈20 KHz and ≈60 s, respectively. The advantages with higher temporal and spectral resolutions are clearly evident in the Gauribidanur observations.

Figure 3 (upper panel) shows the dynamic spectrum of a type III solar radio burst recorded with the instrument on 2014 December 14 during the time interval ≈06:24–06:27 UT. Observations of the same event obtained using the Wind-Waves RAD2 spectrograph are shown in the lower panel of Figure 3 for comparison. This clearly illustrates the excellent temporal correspondence and the near-continuous spectral coverage offered by the two observations. This is important for understanding the characteristics of the solar radio bursts that continue to frequencies <15 MHz in the spectrum and those which do not (see, e.g., the review article by Reid & Ratcliffe 2014).

We found that 12/71 bursts observed with our spectrograph were of comparatively longer duration, >100 s (see Table 4). Among the 12 long-duration bursts, four bursts exhibited quasi-periodicity in their time profile at discrete frequencies. Table 3 lists the dominant periodicities for the four quasi-periodic bursts at a typical frequency (f) like 19.5 MHz (see Section 5 for details). Three of the quasi-periodic bursts occurred in the immediate aftermath of either a partial "halo" or a "halo" coronal mass ejection (CME).[7] The fourth quasi-periodic burst (2014 January 31) was preceded by a "halo"

[6] http://lep694.gsfc.nasa.gov/waves/data_products.html
[7] cdaw.gsfc.nasa.gov

Table 3
Details of the Quasi-periodic Type III Solar Radio Bursts

Date	Burst Time (UT)	Burst Duration (s)	Burst Periodicity p (s)	Magnetic Field B (G)	CME Onset (UT)	CME Width (°)	CME Speed (km s^{-1})
2013 Oct 28	04:36	288	5–75	0.96–0.06	04:07	156	1200
2013 Dec 07	07:22	144	9–61	0.53–0.08	07:01	360	1085
2014 Jan 26	10:09	144	4–28	1.00–0.18	07:53	255	1088
2014 Jan 31	07:26	118	5–29	0.90–0.17	15:36[a]	360	1087

Note.
[a] Previous day.

CME by ≈15 hr. The eight long-duration bursts that did not show any quasi-periodicity were not associated with any 'halo CMEs.

Figure 4 shows the dynamic spectrum of the quasi-periodic bursts observed on 2013 October 28 during the time interval ≈04:36–04:42 UT. The fast drifting features are the characteristic signatures of the group of type III solar radio bursts (Suzuki & Dulk 1985).

Figure 5 shows the time profile (indicated by the solid line) of the group of type III radio bursts in Figure 4 at a typical observing frequency (f) such as 19.5 MHz. Also shown is the time profile of the same event obtained in the total power mode, with only one of the LPDAs in the spectrograph. The dynamic range is about a factor of five higher in the former. This is due to a combination of observations in the correlation mode and an increase in the collecting area (see, e.g., Kraus 1950). The estimation of the visibility amplitude using both the in-phase and quadrature correlations, just as in imaging observations with radio interferometric arrays, and the use of all the cosine and sine components (i.e., $C1$, $C2$, $S1$, and $S2$) to obtain the in-phase and quadrature correlations (see Section 3), further enhance the dynamic range. The latter is particularly useful since the "noise" in the above components is independent. These indicate that the dynamic spectrum of the radio signatures of the transient energy releases in the solar atmosphere can be obtained with better sensitivity through observations in the cross-correlation mode. Note that the presence of quasi-periodicity in the radio emission can be clearly noticed in the correlation mode.

5. ANALYSIS AND RESULTS

The quasi-periodicity in the observed solar radio flux at low frequencies that are primarily from the upper part of the corona is due to the modulation of the electron acceleration/injection process responsible for the radio emission (Aschwanden 1987). The modulation is likely to be communicated on magnetohydrodynamic (MHD) timescales in the acceleration region (Tajima et al. 1987; Aschwanden et al. 1994; Kliem et al. 2000; Asai et al. 2001). In such cases the corresponding Alfvén speed (v_A) can be estimated as

$$v_A \approx \frac{l}{p}, \tag{1}$$

where $l \approx 10{,}000$ km is the typical dimension of the region over which the type III radio burst producing electrons are injected (Lantos et al. 1984; Aschwanden 2002), and p is the observed periodicity. Once v_A is known, the associated magnetic field strength (B) can be calculated using the expression

$$v_A = 2.05 \times 10^6 B N_e^{-1/2}, \tag{2}$$

where N_e is the electron density (corresponding to either f or $f/2$, depending on whether the observed emission corresponds to the fundamental or the harmonic component, respectively) in units of cm^{-3}.

Traditionally the FFT technique is used to estimate the periodicities that may be present in a time domain signal in radio astronomy. But for temporal localization of individual spectral components in a signal, a multi-resolution analysis is considered to be a better approach. The wavelet transform technique offers this advantage (Kaiser 1994; Torrence & Compo 1998; Zaqarashvili et al. 2013).

Figure 6 shows the wavelet power spectrum for the radio burst in Figure 5 (correlation mode). A wide range of periodicities can be seen in the spectrum. The duration of each one of them is shown in Figure 7. Considering only those periodicities within the $1/e$ width of the "fit" to the data points in Figure 7, we find that $p \approx 5$–75 s. Note that the above $1/e$ region includes nearly all the periodicities outside the cone of influence (COI) boundary of the wavelet transform in Figure 6. The magnetic field strengths (corresponding to the above values of p) estimated using Equations (1) and (2) are in the range $B \approx 0.96$–0.06 G. Interestingly, the estimates for the other three events are also nearly the same (see Table 3). This adds confidence to our results. We have assumed that the quasi-periodic radio bursts in Table 3 are due to second harmonic plasma emission since the viewing angle of the sunspot active regions associated with all the bursts is $\gtrsim 30°$. Furthermore, the fundamental plasma emission is more directive at low frequencies (Suzuki & Sheridan 1982).

The multiple periodicities in each event listed in Table 3 indicate that the observed quasi-periodic pulsations are possibly due to the interaction of different magnetic structures (see, e.g., Tomczak & Sfaforz 2014). Each pulsation corresponds to a burst of electron acceleration in a reconnection region. The episodes of acceleration/reconnection occur at different locations, but are triggered by a common phenomenon (Benz 1994). Note that the probability of interaction and reconnection between an expanding CME and the neighboring open magnetic field structures, leading to the generation of groups of type III radio bursts, is also very high (see, e.g., Murray et al. 2007). The applicability of the above arguments to the present case is further strengthened by the reports that there is large-scale reconfiguration of the coronal magnetic field (which facilitates reconnection) in the aftermath of a "halo" CME. The time period over which this occurs is $\lesssim 19$ hr (Hansen et al. 1974; Hiei et al. 1993; Kathiravan et al. 2007).

Table 4
List of Radio Bursts Observed with the Spectrograph

No.	Date	Time (UT)	Duration (s)
1	2013 Oct 18	07:08	12
2	2013 Oct 20	04:33	18
3	⋯	05:20	14
4	⋯	05:34	18
5	⋯	05:45	25
6	⋯	06:52	21
7	⋯	06:57	18
8	⋯	07:23	115
9	2013 Oct 21	05:11	19
10	⋯	06:21	7
11	⋯	06:44	17
12	⋯	07:29	18
13	⋯	08:08	12
14	⋯	08:35	100
15	⋯	09:22	57
16	2013 Oct 23	09:56	20
17	⋯	05:12	30
18	⋯	07:49	28
19	2013 Oct 28	04:36	288
20	2013 Nov 02	04:44	36
21	⋯	06:03	23
22	⋯	06:19	18
23	⋯	06:48	33
24	2013 Nov 05	06:00	36
25	2013 Nov 07	03:38	12
26	2013 Nov 20	05:49	108
27	2013 Nov 21	07:31	11
28	2013 Nov 23	08:45	14
29	2013 Nov 24	06:06	25
30	2013 Nov 28	08:14	7
31	2013 Dec 04	05:12	14
32	2013 Dec 05	05:36	16
33	⋯	06:36	25
34	2013 Dec 07	07:22	144
35	2013 Dec 14	03:06	18
36	⋯	06:24	72
37	⋯	07:07	43
38	⋯	08:21	21
39	2013 Dec 15	04:21	19
40	⋯	06:30	14
41	⋯	07:13	25
42	⋯	08:15	18
43	⋯	10:30	58
44	2013 Dec 16	06:58	7
45	⋯	07:24	2
46	2013 Dec 23	06:27	18
47	2013 Dec 26	05:08	18
48	⋯	05:58	64
49	2013 Dec 28	07:02	216
50	2013 Dec 30	04:01	12
51	⋯	05:54	46
52	⋯	07:49	104
53	⋯	08:06	23
54	2014 Jan 18	04:35	108
55	2014 Jan 24	08:07	21
56	2014 Jan 26	10:09	144
57	2014 Jan 27	05:24	14
58	⋯	06:02	32
59	⋯	07:49	7
60	2014 Jan 28	05:31	63
61	⋯	06:06	7
62	⋯	07:28	237
63	⋯	09:34	9
64	⋯	09:36	6
65	2014 Jan 29	04:18	64
66	⋯	07:28	27
67	2014 Jan 30	06:06	14
68	2014 Jan 31	05:42	108
69	⋯	07:25	118
70	2014 Feb 02	09:29	20
71	2014 Feb 03	04:45	21

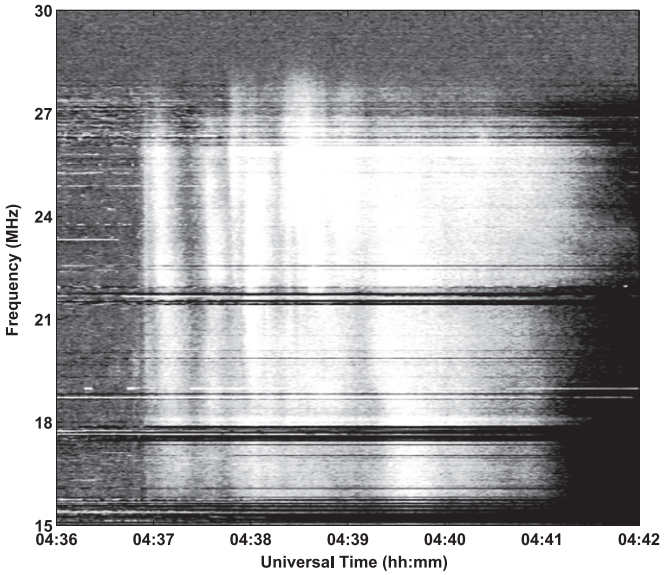

Figure 4. Dynamic spectrum of the group of type III solar radio bursts observed on 2013 October 28 during the interval ≈04:36–04:42 UT. The dark patch toward the end of the observations is due to sudden ionospheric disturbance' (commonly referred to as "short-wave fadeout") in the Earth's ionosphere.

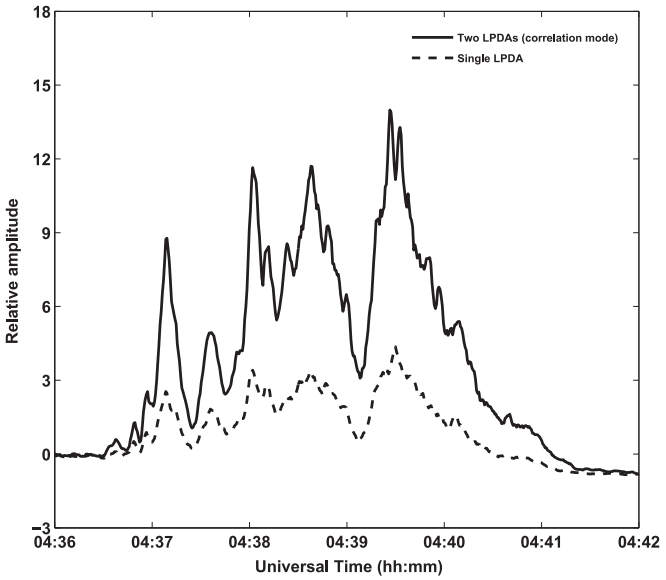

Figure 5. Comparison of the time profiles of the group of type III bursts (in Figure 4) as obtained with the two LPDAs (correlation mode) and a single LPDA (total power mode), at 19.5 MHz.

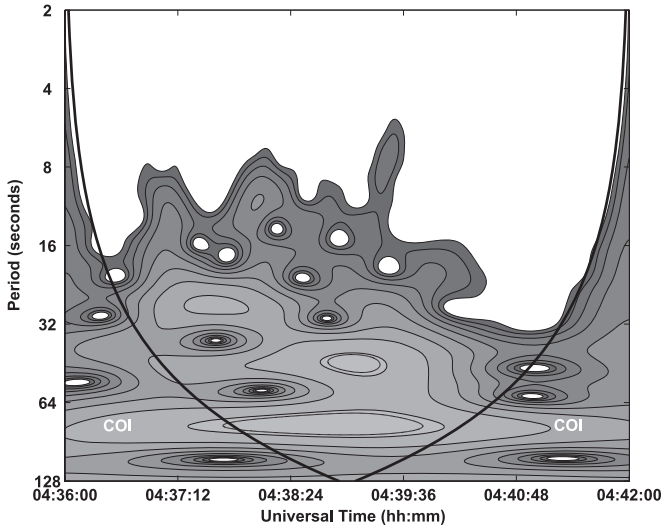

Figure 6. Wavelet spectrum for the 19.5 MHz correlation mode time profile in Figure 5. The region marked COI is the "cone of influence" in which the edge effects become important due to the limited time series data and have a higher contribution of artifacts. Portions of the spectrum present within the COI, as well as close to either side of its boundary, should be treated with caution because of the aforementioned reason (see, e.g., Torrence & Compo 1998).

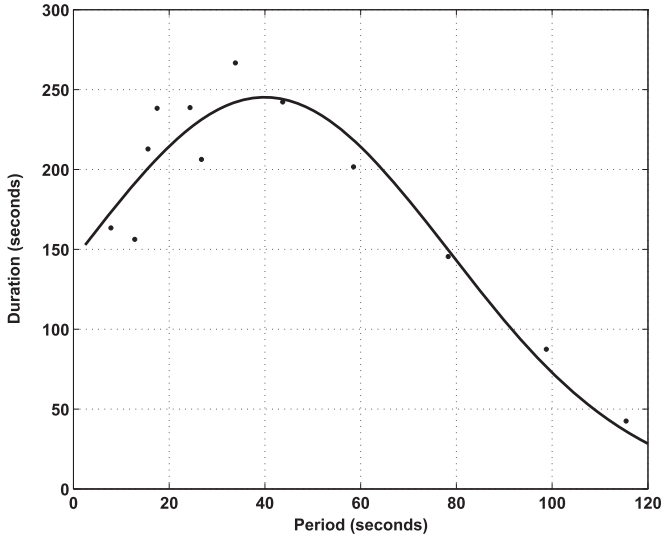

Figure 7. Distribution of the duration of the different periodicities outside the COI in Figure 6, obtained by taking horizontal slices through the latter. The dashed line is the "fit" to the estimated periodicities.

The upper limit of the above period is nearly the same as the period (≈20 hr) reported by Tsuneta et al. (1992) in the context of global restructuring of the corona due to magnetic reconnections after the disappearance of a polar crown filament. Interestingly the latter is usually associated with the CMEs. Therefore multiple magnetic reconnections in the aftermath of either the partial "halo" or "halo" CMEs could be the cause of the quasi-periodicity for the four long-duration bursts listed in Table 3 because: (1) neither partial "halo" nor "halo" CMEs were associated with the other eight long-duration bursts that did not show any quasi-periodicity (see Section 4); (2) statistical results show that the group of type III bursts observed at low frequencies are always preceded by CMEs of width >140° (Cane et al. 2002). The rapid and irregular variations in the peak amplitudes of the pulsations point to a bursty, time-dependent reconnection process in the present case (see, e.g., Kliem et al. 2000; Aschwanden 2004, p. 407). An estimate of the v_A values (using Equation (1)) corresponding to a range of periodicities for each event listed in Table 3 indicates that the spread in the former agrees well with the coalescence speeds (≈200–2000 km s^{-1}) of the magnetic islands that lead to the burst of electron acceleration in the above reconnection process (Aschwanden 2002). These imply that radio observations of quasi-periodic pulsations could be a useful tool for estimating the coronal plasma parameters in the reconnection/electron acceleration regions.

6. SUMMARY

A low-frequency (30–15 MHz) spectro-correlator for solar observations was recently commissioned at the Gauribidanur Observatory using high-speed digitizer and FPGA hardware for the backend instrumentation. Observations indicate that the dynamic range is higher than that obtained using conventional techniques. Located at ≈77°E 13°N, the above instrument provides the possibility of having continuous observations of the Sun for ≈15 hr in a day (at present), along with other similar low-frequency spectrographs located at other terrestrial longitudes. We are exploring the possibility of carrying out continuous observations for more than 15 hr a day. Moreover, it minimizes the spectral gap with the Wind-Waves observations. There are also other advantages such as (1) the above local latitude being within the declination range (−23°S to +23°N) over which the Sun moves in a year[8]; and (2) Gauribidanur is relatively radio "quiet" (Monstein et al. 2007); furthermore, the ionospheric cutoff frequency is comparable to or better than that elsewhere (Zucca et al. 2012; Zaqarashvili et al. 2013; Lecacheux et al. 2014; Tun et al. 2015); (3) the digital signal processing techniques, higher temporal resolution, and the cross-correlation mode of operation help to to detect the quasi-periodicities in the time profiles with good contrast[9]; (4) there is a possibility that the ionospheric cutoff frequency for radio wave propagation might decrease in the coming years because of the steady decline in the solar and the interplanetary magnetic fields in the ongoing solar cycle, (solar cycle 24), and predictions of a weak future solar cycle (solar cycle 25; see, e.g., Janardhan et al. 2015 and the references therein). Since the antenna and the receiver system described in the present work can be easily reconfigured to observe at frequencies <15 MHz, we should be able to achieve spectral overlap with Wind-Waves observations. We also intend to extend the observations on the high-frequency side to have continuous spectral coverage up to ≈100 MHz. The data rate should not be a problem since standalone FPGA systems with fast ADCs and facilities for on board processing are available.[10]

Wavelet analyses of the group of long-duration (>100 s) type III solar radio bursts observed with our spectrograph indicate that those which are preceded by either partial "halo" or "halo" CMEs are quasi-periodic with periodicities in the range $p \approx 4$–75 s at a typical frequency such as 19.5 MHz. The coronal magnetic field strengths calculated using the above periodicities are in the range $B \approx 1.00$–0.06 G. Note that radio

[8] http://www.arcetri.astro.it/~kreardon/EGSO/gbo/observatories.html
[9] http://www.astro.umd.edu/~white/gb/Data/Images/2013/10/28/20131028_042500_BIRS.png
[10] http://www.xilinx.com/univ/xupv5-lx110t.htm

emission at low frequencies originate typically in the "middle" corona ($1.2\ R_\odot \lesssim r \lesssim 3\ R_\odot$) where r is the heliocentric distance. Observations over the above range of r at other frequency bands in the electromagnetic spectrum are presently limited. Hence radio observations similar to those reported in the present work could be an effective tool for routine monitoring and seismology in the aforementioned region of the solar atmosphere to understand the plasma parameters there. A number of scientific problems, e.g., the CME-solar energetic protons (SEP)-low-frequency type III burst (type III-l) association in the context of Space Weather studies, can also be investigated (MacDowall et al. 2003; Cliver & Ling 2009). Additionally, the corona overlying the visible solar disk well off its limb can be simultaneously observed; and weak energy releases in the solar atmosphere can be observed with good contrast via the associated non-thermal radio emission (Benz 1995; Li et al. 2009). Finally, the cross-correlation scheme described in this work can also be successfully extended to observations of non-solar transients.

We thank the staff of the Gauribidanur Observatory for their help with data acquisition, fabrication of the antennas/receiver systems, and their maintenance. The work was carried out when one of the authors (Abhilash HN) was a Visiting Intern at the Indian Institute of Astrophysics. We are grateful to the referee for kind comments that helped us to present the results more clearly. S.M. White and the NASA-GSFC/Wind-Waves team are thanked for providing open access to the Bruny Island Radio Spectrometer and Wind-Waves observations, respectively.

REFERENCES

Asai, A., Shimojo, M., Isobe, H., et al. 2001, ApJL, 562, L103
Aschwanden, M. J. 1987, SoPh, 111, 113
Aschwanden, M. J. 2002, SSRv, 101, 1
Aschwanden, M. J. 2004, Physics of the Solar Corona (Berlin: Springer)
Aschwanden, M. J., Benz, A. O., & Montello, M. L. 1994, ApJ, 431, 432
Baan, W. A., Fridman, P. A., & Millenaar, R. P. 2004, AJ, 128, 933
Balanis, C. A. 2005, Antenna Theory: Analysis and Design (New Delhi: Wiley)
Bastian, T. S. 2004, P&SS, 52, 1381
Benz, A. O. 1994, SSRv, 68, 135
Benz, A. O. 1995, in Coronal Magnetic Energy Releases, ed. A. O. Benz, & A. Krüger, Vol. 444 (Berlin: Springer), 1
Benz, A. O., Monstein, C., Meyer, H., et al. 2009, EM&P, 104, 277
Boischot, A., Rosolen, C., Aubier, M. G., et al. 1980, Icar, 43, 399
Bougeret, J.-L., Kaiser, M. L., Kellogg, P. J., et al. 1995, SSRv, 71, 5
Cane, H. V., & Erickson, W. C. 2005, ApJ, 623, 1180
Cane, H. V., Erickson, W. C., & Prestage, N. P. 2002, JGR, 107, 14
Carley, E. P., Reid, H. A. S., Vilmer, N., & Gallagher, P. T. 2015, A&A, 581, A100
Cliver, E. W., & Ling, A. G. 2009, ApJ, 690, 598
Duhamel, R. H., & Isbell, D. E. 1957, IRE Nat. Conv. Rec., Part I, 119
Eastwood, J. P., Wheatland, M. S., Hudson, H. S., et al. 2010, ApJL, 708, L95
Ebenezer, E., Ramesh, R., Subramanian, K. R., SundaraRajan, M. S., & Sastry, Ch. V. 2001, A&A, 367, 1112
Ebenezer, E., Subramanian, K. R., Ramesh, R., SundaraRajan, M. S., & Kathiravan, C. 2007, BASI, 35, 111
Erickson, W. C. 1997, PASA, 14, 278
Gopalswamy, N., Aguilar-Rodriguez, E., Yashiro, S., et al. 2005, JGR, 110, A12S07
Gopalswamy, N., Kaiser, M. L., Lepping, R. P., et al. 1998, JGR, 103, 307
Gopalswamy, N., & Mäkelä, P. 2010, ApJL, 721, L62
Hansen, R. T., Garcia, C. J., Hansen, S. F., & Yasukawa, E. 1974, PASP, 86, 500
Hiei, E., Hundhausen, A. J., & Sime, D. G. 1993, GeoRL, 20, 2785
Isbell, D. E. 1960, ITAP, AP-8, 260
Iwai, K., Tsuchiya, F., Morioka, A., & Misawa, H. 2012, SoPh, 277, 447
Janardhan, P., Bisoi, S. K., Ananthakrishnan, S., et al. 2015, JGRA, 120, 5306
Kaiser, G. 1994, A Friendly Guide to Wavelets (Boston: Birkhäuser)
Kathiravan, C., Ramesh, R., & Nataraj, H. S. 2007, ApJL, 656, L40
Kishore, P., Kathiravan, C., Ramesh, R., Barve, Indrajit V., & Rajalingam, M. 2014, SoPh, 289, 3995
Kishore, P., Ramesh, R., Kathiravan, C., & Rajalingam, M. 2015, SoPh, 290, 2409
Kliem, B., Karlický, M., & Benz, A. O. 2000, A&A, 360, 715
Kraus, J. D. 1950, Radio Astronomy (New York: McGraw-Hill)
Lantos, P., Pick, M., & Kundu, M. R. 1984, ApJL, 283, L71
Leblanc, Y., Dulk, G. A., Vourlidas, A., & Bougeret, J.-L. 2001, JGR, 106, 25301
Lecacheux, A., Konovalenko, A. A., & Rucker, H. O. 2014, P&SS, 52, 1357
Li, B., Cairns, I. H., & Robinson, P. A. 2009, JGR, 114, A02104
MacDowall, R. J., Lara, A., Manoharan, P. K., et al. 2003, GeoRL, 30, 8010
McLean, D. J., & Labrum, N. R. 1985, Solar Radiophysics (Cambridge: Cambridge Univ. Press)
Melnik, V. N., Brazhenko, A. I., Konovalenko, A. A., et al. 2014, SoPh, 289, 263
Mercier, C., & Trottet, G. 1997, ApJL, 474, L65
Monstein, C., Ramesh, R., & Kathiravan, C. 2007, BASI, 35, 473
Morioka, A., Miyoshi, Y., Masuda, S., et al. 2007, ApJ, 657, 567
Morosan, D. E., Gallagher, P. T., Zucca, P., et al. 2014, A&A, 568, A67
Murray, M. J., van Driel-Gesztelyi, L., Démoulin, P., et al. 2007, SoPh, 240, 283
Oberoi, D., Matthews, L. D., Cairns, I. H., et al. 2011, ApJL, 728, L27
Prestage, N. P. 1995, JATP, 57, 1815
Ramesh, R. 2011, in Proc. Astron. Soc. India Conf. Ser., Vol. 2, First Asia-Pacific Solar Physics Meeting, ed. A. R. Choudhuri, & D. Banerjee (Bangalore: ASI), 55
Ramesh, R., Annalakshmi, M., Kathiravan, C., Gopalswamy, N., & Umapathy, S. 2012, ApJ, 752, 107
Ramesh, R., & Ebenezer, E. 2001, ApJL, 558, L141
Ramesh, R., Kathiravan, C., Barve, Indrajit V., Beeharry, G. K., & Rajasekara, G. N. 2010a, ApJ, 719, 41
Ramesh, R., Kathiravan, C., Kartha, Sreeja S., & Gopalswamy, N. 2010b, ApJ, 712, 188
Ramesh, R., Kathiravan, C., & SatyaNarayanan, A. 2011, ApJ, 734, 39
Ramesh, R., Kathiravan, C., SatyaNarayanan, A., & Ebenezer, E. 2003, A&A, 400, 753
Ramesh, R., Sasikumar Raja, K., Kathiravan, C., & SatyaNarayanan, A. 2013, ApJ, 762, 89
Ramesh, R., SatyaNarayanan, A., Kathiravan, C., Sastry, Ch. V., & UdayaShankar, N. 2005, A&A, 431, 353
Ramesh, R., Subramanian, K. R., SundaraRajan, M. S., & Sastry, Ch. V. 1998, SoPh, 181, 439
Ramesh, R., SundaraRajan, M. S., & Sastry, Ch. V. 2006, ExA, 21, 31
Ratcliffe, H., Kontar, E. P., & Reid, H. A. S. 2014, A&A, 572A, 111
Reid, H. A. S., & Kontar, E. P. 2015, A&A, 577A, 124
Reid, H. A. S., & Ratcliffe, H. 2014, RAA, 14, 773
Reiner, M. J., Fainberg, J., Kaiser, M. L., & Bougeret, J.-L. 2007, SoPh, 241, 351
Roberts, B., Edwin, P. M., & Benz, A. O. 1984, ApJ, 279, 857
Ryabov, V. B., Vavriv, D. M., Zarka, P., et al. 2010, A&A, 510, A16
SasikumarRaja, K., Kathiravan, C., Ramesh, R., Rajalingam, M., & Barve, Indrajit V. 2013, ApJS, 207, 2
SasikumarRaja, K., & Ramesh, R. 2013, ApJ, 775, 38
ShanmughaSundaram, G. A., & Subramanian, K. R. 2004, SoPh, 222, 311
Suzuki, S., & Dulk, G. A. 1985, in Solar Radiophysics, ed. D. J. McLean, & N. R. Labrum (Cambridge: Cambridge Univ. Press), 320
Suzuki, S., & Sheridan, K. V. 1982, PASAu, 4, 382
Tajima, T., Sakai, J., Nakajima, H., et al. 1987, ApJ, 321, 1031
Taylor, G. B., Ellingson, S. W., Kassim, N. E., et al. 2012, JAI, 1, 1250004
Tomczak, M., & Sfaforz, S. 2014, CEAB, 38, 111
Torrence, C., & Compo, G. P. 1998, BAMS, 79, 61
Tsuneta, S., Takahashi, T., Acton, L. W., et al. 1992, PASJ, 44L, 211
Tun, S. B., Cutchin, S., & White, S. M. 2015, arXiv:1508.00206
Zaqarashvili, T. V., Melnik, V. N., Brazhenko, A. I., et al. 2013, A&A, 555, A55
Zhao, R.-y., Mangeney, A., & Pick, M. 1991, A&A, 241, 183
Zucca, P., Carley, E. P., McCauley, J., et al. 2012, SoPh, 280, 591